

The parity determination of the pentaquark Θ^+ from photoproduction near threshold

Byung Geel Yu,^{1,2,*} Tae Keun Choi,^{3,†} and Chueng-Ryong Ji^{2,‡}

¹*Department of General studies, Hangeong Aviation University, Koyang, 200-1, Korea*

²*Department of Physics, North Carolina State University,
Raleigh, North Carolina 27695-8202, USA*

³*Department of Physics, Yonsei University, Wonju, 220-710, Korea*

(Dated: May 23, 2019)

Abstract

We discuss how the differential cross section near threshold for the reaction $\gamma N \rightarrow K\Theta^+$ can be an important tool to determine the parity of the Θ^+ in a model-independent way. Using the CGLN amplitudes, we present a justification to our description. We extend our analysis to the photon polarization asymmetry which can play an important role in determining the Θ^+ parity without ambiguity.

PACS numbers: 13.40.-f, 13.60.Rj, 13.75.Jz, 13.88.+e

*Electronic address: bgyu@mail.hangeong.ac.kr

†Electronic address: tkchoi@dragon.yonsei.ac.kr

‡Electronic address: crji@unity.ncsu.edu

The discovery of the pentaquark Θ^+ baryon [1, 2, 3, 4, 5, 6, 7, 8] opens the new realm of investigating hadron structures that are beyond the scope of the conventional quark models. The mass and decay width of the Θ^+ estimated from the experiments are consistent with theoretical predictions of the chiral soliton model [9] within the experimental uncertainty. Also the quantum numbers such as the spin $\frac{1}{2}$ and isospin singlet with positive strangeness $s = +1$ tend to be established from the analysis of experimental data [7, 10]. However, the parity of the Θ^+ is still a controversial issue [11, 12]. Concerning the parity of the Θ^+ , there has been a series of the theoretical approaches to determine the parity of the Θ^+ from the photo- and meson-induced productions of the Θ^+ directly [13, 14, 15, 16, 17, 18, 19, 20]. These approaches were initially focusing on the model predictions for the cross sections of the SAPHIR and CLAS experiments and some results favored the positiveness of the Θ^+ parity. However, based on the reanalyses of the K^+d and K^+p scattering data [21, 22], the uncertainty in the decay width of the Θ^+ due to the limited resolution of the experiments are under discussion. From the more theoretical ground [23, 24], some suspected that the cross section of the SAPHIR data may be retracted by an order of magnitude smaller than claimed in Ref. [2]. Moreover, as we discussed before [13], there is a wide theoretical uncertainty in the model calculations associated with the different assumption on the gauge prescription as well as the cutoff Λ [13, 14, 15, 16, 20]. Thus, at the current situation, it is not at all clear which sign of the Θ^+ parity is the correct one.

In this letter we present a reasoning why the angular distribution of the Θ^+ photoproduction near threshold is an effective tool to distinguish the parity of the Θ^+ . We will demonstrate that the first principle conservation laws give strong constraints on the differential cross sections near threshold and consequently the features of the differential cross sections between the two opposite parity states are clearly distinguishable.

Before we apply the conservation laws of the parity and angular momentum to $\gamma N \rightarrow K\Theta^+$, we first summarize our reasoning why the total cross sections alone may not be so effective in the determination of the Θ^+ parity. In Fig. 1, the cross sections for $\gamma N \rightarrow K\Theta^+$ were obtained using the pseudovector(PV) coupling for the $KN\Theta^+$ interaction with the coupling constant $g_{KN\Theta}$ taken from the width $\Gamma_{\Theta^+} = 5$ MeV for both parities [13]. The coupling constants used in the calculation are listed in Table I and the Θ^+ magnetic moment is taken as $\kappa_{\Theta} = 0$ for simplicity. The details of the gauge prescription and the associated form factors were presented in our previous work [13].

As can be seen in Fig. 1, the positive and negative parity cases give the total cross sections of the order of 100 nb and 10 nb, respectively. However the current experimental results are not exactly clear about which order of the magnitude, i.e. 100 nb or 10 nb, is the correct one. Thus, we

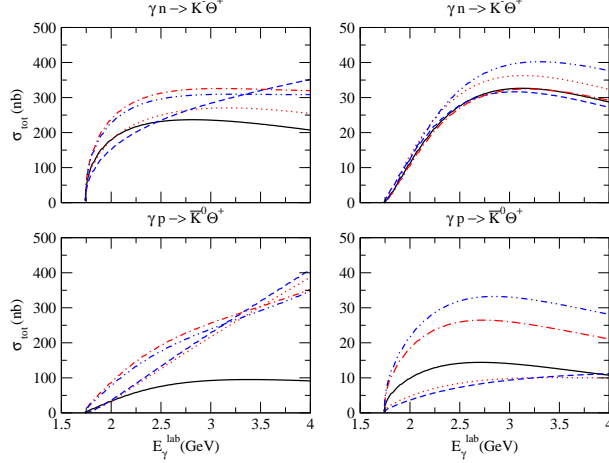


FIG. 1: Total cross sections of the $\Theta^+(\frac{1}{2}^+)$ (left column) and $\Theta^+(\frac{1}{2}^-)$ (right column) for $\gamma N \rightarrow K\Theta^+$ in the PV coupling scheme. The solid lines are the contributions of the Born terms with $g_{KN\Theta} = 2.2(0.3)$ and $g_{K^*N\Theta} = 0$. The dotted lines are the sum of the Born terms and K^* with $g_{K^*N\Theta} = 1.32(0.18)$. The dot-dashed lines are the sum of the Born terms and K^* with $g_{K^*N\Theta} = -1.32(-0.18)$. The dashed lines are the sum in total of the Born terms, K^* and K_1 with $g_{K^*N\Theta} = 1.32$, $g_{K_1N\Theta} = -0.07(-0.1)$ for $\gamma n \rightarrow K^-\Theta^+(\gamma p \rightarrow \bar{K}^0\Theta^+)$ for $\Theta^+(\frac{1}{2}^+)$ and $g_{K^*N\Theta} = 0.18$, $g_{K_1N\Theta} = -0.1(-0.16)$ for $\gamma n \rightarrow K^-\Theta^+(\gamma p \rightarrow \bar{K}^0\Theta^+)$ for $\Theta^+(\frac{1}{2}^-)$. The dot-dot-dashed lines are the sum in total of the Born terms, K^* and K_1 with $g_{K^*N\Theta} = -1.32$, $g_{K_1N\Theta} = +0.07(+0.1)$ for $\gamma n \rightarrow K^-\Theta^+(\gamma p \rightarrow \bar{K}^0\Theta^+)$ for $\Theta^+(\frac{1}{2}^+)$ and $g_{K^*N\Theta} = -0.18$, $g_{K_1N\Theta} = +0.1(+0.16)$ for $\gamma n \rightarrow K^-\Theta^+(\gamma p \rightarrow \bar{K}^0\Theta^+)$ for $\Theta^+(\frac{1}{2}^-)$.

think that it is necessary to go beyond the total cross sections and investigate the differential cross sections for the discrimination of the Θ^+ parity [13]. Although the hadron model involves several unknown parameters, we notice that such model dependence can be minimized in the analysis near threshold because only the lower angular momentum states are available and thus it is rather easy to implement the first principle conservation laws [25].

In order to apply the conservation laws of parity and angular momentum to $\gamma N \rightarrow K\Theta^+$, the inspection of the reaction specific to the threshold energy is necessary. Let us make it clear that the relevant kinematics near threshold energy is rather simple. Near threshold, we can assume in the final $K\Theta^+$ state that the kaon angular momentum $l_K = 0$ or 1, since $|\mathbf{q}|R \approx \sqrt{l_K(l_K + 1)} \leq 2$ up to a few hundred MeV/c for the kaon momentum in the center of mass frame with R , a typical hadronic scale of one fermi. Thus the total spin of the final state is $J_f = \frac{1}{2}$ or $\frac{3}{2}$. In the case of $l_K = 0$ and $J_f = \frac{1}{2}$, the total parity of the final state has two options; (i) $P_f = -1$, if the parity of the Θ^+ taken positive or (ii) $P_f = +1$, if the parity of the Θ^+ taken negative. For the case of $l_K = 1$, the above options of the Θ^+ parity should be reversed. On the other hand, the photon

TABLE I: Coupling constants used in the calculation for $\gamma N \rightarrow K\Theta^+$. $\Gamma_{\Theta^+ \rightarrow NK} = 5$ MeV taken for $g_{KN\Theta}$ of the $\Theta^+(\frac{1}{2}^\pm)$ [13]. References are from ^athe assumption [15], ^bPDG [26], ^c $\gamma p \rightarrow K^+\Lambda$ [27] where we assume $\frac{G_{K^*N\Theta}}{G_{K_1N\Theta}} \simeq \frac{G_{K^*N\Lambda(1116)}}{G_{K_1N\Lambda(1116)}}$ for $\Theta^+(\frac{1}{2}^+)$ and $\frac{G_{K^*N\Theta}}{G_{K_1N\Theta}} \simeq \frac{G_{K^*N\Lambda(1405)}}{G_{K_1N\Lambda(1405)}}$ for $\Theta^+(\frac{1}{2}^-)$ with $G_{K^*(K_1)NY} = g_{K^*(K_1)K\gamma}g_{K^*(K_1)NY}$, and ^d $\Gamma_{K_1K\rho} = 37.8$ MeV with Vector Dominance $g_{K_1K\gamma} = \frac{e}{f_\rho}g_{K_1K\rho}$ [28]. Values in the parenthesis are denoted by $\gamma n \rightarrow K^-\Theta^+(\gamma p \rightarrow \bar{K}^0\Theta^+)$ respectively.

	Positive parity	Negative parity	References
$g_{KN\Theta}$	2.2	0.3	$\Gamma_{\Theta^+ \rightarrow NK}$
$g_{K^*N\Theta}$	± 1.32	± 0.18	$\frac{g_{K^*N\Theta}}{g_{KN\Theta}} = 0.6^a$
$g_{K^*K\gamma}$	0.254(0.388)	0.254(0.388)	$\Gamma_{K^* \rightarrow K\gamma}^b$
$g_{K_1N\Theta}$	$\mp 0.07(0.1)$	$\mp 0.1(0.16)$	$\frac{G_{K^*N\Lambda(1116)}}{G_{K_1N\Lambda(1116)}} \simeq -8^c$ $\frac{G_{K^*N\Lambda(1405)}}{G_{K_1N\Lambda(1405)}} \simeq -0.7^c$
$g_{K_1K\gamma}$	0.6	0.6	$g_{K_1K\rho}^d$

orbital angular momentum near threshold must have $l_\gamma = 0$ in order for the total spin of the initial state γN to have $J_i = \frac{3}{2}$ or $\frac{1}{2}$ by the conservation of the total angular momentum. Then, the total parity of the initial state $P_i = -1$ is given uniquely. Therefore, following the parity conservation, the final state should have $l_K = 0$ with $P_f = -1$, i.e., the s-wave kaon production near threshold when the Θ^+ has the positive parity. Similarly, the angular momentum and parity of the final state should be $l_K = 1$ with $P_f = -1$ for the negative parity of the Θ^+ . Thus the p-wave kaon production is expected near threshold when the parity of Θ^+ is negative.

In Figs. 2 and 3, the angular distributions of $\gamma n \rightarrow K^-\Theta^+$ and $\gamma p \rightarrow \bar{K}^0\Theta^+$ in the PV coupling scheme are presented, respectively. As illustrated above, the solid line of $\gamma n \rightarrow K^-\Theta^+$ near threshold, i.e. at $E_\gamma = 1.8$ GeV, shows the typical s-wave kaon production of the Born terms for $\Theta^+(\frac{1}{2}^+)$ and the p-wave distribution of the Born terms for $\Theta^+(\frac{1}{2}^-)$ respectively. The angular distributions of $\gamma p \rightarrow \bar{K}^0\Theta^+$ displayed by the solid lines in Fig. 3 are also the consequences of the conservation of parity and angular momentum. Note that our Born contributions to the angular distributions for $\Theta^+(\frac{1}{2}^+)$ in Figs. 2 and 3 agree with those(dotted lines of Fig.10) in Ref. [16]. Although, there is some model dependence especially due to the K^* and K_1 contributions, the distinction between the positive and negative parities is quite clear and it is not degraded by the model dependence. Therefore, the angular distributions near threshold should be the useful informations to the parity of the Θ^+ . To reduce the model dependence arising from the form factors further, we presented the normalized differential cross sections divided by the total cross section.

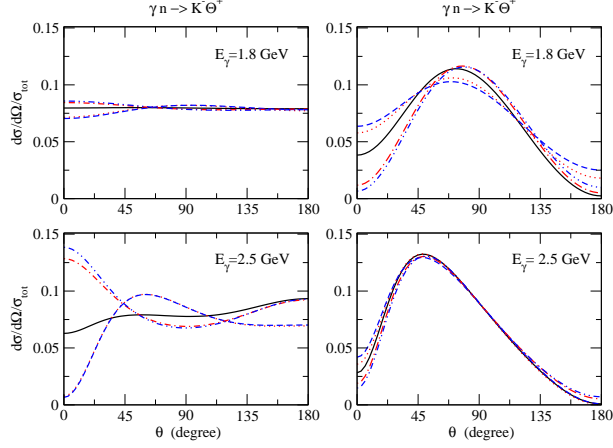


FIG. 2: Normalized differential cross sections $\frac{1}{\sigma} \frac{d\sigma}{d\Omega}$ of the $\Theta^+(\frac{1}{2}^+)$ (left) and the $\Theta^+(\frac{1}{2}^-)$ (right) for $\gamma n \rightarrow K^- \Theta^+$ at $E_\gamma = 1.8$ and 2.5 GeV. The notations are the same as Fig. 1.

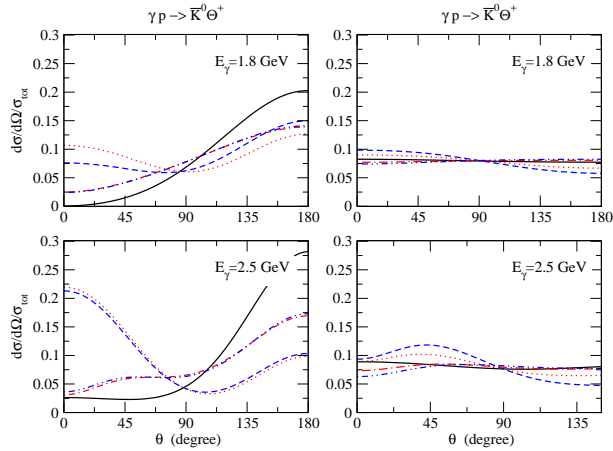


FIG. 3: Normalized differential cross sections $\frac{1}{\sigma} \frac{d\sigma}{d\Omega}$ of the $\Theta^+(\frac{1}{2}^+)$ (left) and the $\Theta^+(\frac{1}{2}^-)$ (right) for $\gamma p \rightarrow \bar{K}^0 \Theta^+$ at $E_\gamma = 1.8$ and 2.5 GeV. The notations are the same as Fig. 1.

To convince ourselves further, let us expand the photoproduction operator in terms of the CGLN amplitudes [29]. In the case of $\Theta^+(\frac{1}{2}^+)$,

$$\mathbf{J}^+ \cdot \boldsymbol{\epsilon}_\lambda = F_1^+ i\boldsymbol{\sigma} \cdot \hat{\boldsymbol{\epsilon}}_\lambda + F_2^+ \boldsymbol{\sigma} \cdot \hat{\mathbf{q}} \boldsymbol{\sigma} \cdot (\hat{\boldsymbol{\epsilon}}_\lambda \times \hat{\mathbf{k}}) + F_3^+ i\boldsymbol{\sigma} \cdot \hat{\mathbf{k}} \hat{\mathbf{q}} \cdot \hat{\boldsymbol{\epsilon}}_\lambda + F_4^+ i\boldsymbol{\sigma} \cdot \hat{\mathbf{q}} \hat{\mathbf{q}} \cdot \hat{\boldsymbol{\epsilon}}_\lambda, \quad (1)$$

where $\hat{\mathbf{k}}$, $\hat{\mathbf{q}}$ are the unit vectors of photon and kaon three momenta and $\hat{\boldsymbol{\epsilon}}_\lambda$ is the photon polarization vector. Likewise, the expansion of the photoproduction operator for the $\Theta^+(\frac{1}{2}^-)$ is given by

$$\mathbf{J}^- \cdot \boldsymbol{\epsilon}_\lambda = F_1^- i\boldsymbol{\sigma} \cdot (\hat{\boldsymbol{\epsilon}}_\lambda \times \hat{\mathbf{k}}) + F_2^- \boldsymbol{\sigma} \cdot \hat{\mathbf{q}} \boldsymbol{\sigma} \cdot \hat{\boldsymbol{\epsilon}}_\lambda + F_3^- i\boldsymbol{\sigma} \cdot (\hat{\mathbf{q}} \times \hat{\mathbf{k}}) \hat{\mathbf{q}} \cdot \hat{\boldsymbol{\epsilon}}_\lambda + F_4^- \hat{\mathbf{q}} \cdot \hat{\boldsymbol{\epsilon}}_\lambda. \quad (2)$$

The superscripts \pm stand for the parities of the Θ^+ in what follows. The CGLN amplitudes in

Eqs. (1) and (2) are given by

$$\begin{aligned}
F_1^\pm &= \frac{|\mathbf{k}|}{4\pi} N_+ \left[A_1^\pm \mp \frac{1}{2}(W \pm M)A_3^\pm \mp \frac{p' \cdot k}{W \mp M} A_4^\pm \right], \\
F_2^\pm &= \mp \frac{|\mathbf{k}|}{4\pi} N_- \left[\pm A_1^\pm + \frac{1}{2}(W \mp M)A_3^\pm + \frac{p' \cdot k}{W \pm M} A_4^\pm \right], \\
F_3^\pm &= \mp \frac{|\mathbf{k}||\mathbf{q}|}{4\pi} N_\pm \left[(W - M)A_2^\pm - A_4^\pm \right], \\
F_4^\pm &= \pm \frac{|\mathbf{k}||\mathbf{q}|}{4\pi} N_\mp \left[(W + M)A_2^\pm + A_4^\pm - \frac{(W + M)\mathbf{k} \cdot \mathbf{q}}{(E + M)(E_\Theta + M_\Theta)} \left(A_2^- - \frac{A_4^-}{W - M} \right) \right], \quad (3)
\end{aligned}$$

with the normalization constant $N_\pm = \sqrt{\frac{E_\Theta \pm M_\Theta}{2W}}$. The invariant amplitudes A_i^\pm 's of the PV coupling scheme for the nucleon spinor (p, n) are then given by

$$\begin{aligned}
A_1^\pm &= eg_{KN\Theta} \left[\frac{F_1(s)(\frac{1}{2}(1 + \tau_3) + \kappa_N)}{s - M^2} + \frac{F_2(u)(1 \pm \kappa_\Theta)}{u - M_\Theta^2} \right] \pm \frac{eg_{KN\Theta}}{M_\Theta \pm M} \left(F_1(s) \frac{\kappa_N}{2M} + F_2(u) \frac{\kappa_\Theta}{2M_\Theta} \right), \\
A_2^\pm &= \frac{-2eg_{KN\Theta} \hat{F}}{X(u - M_\Theta^2)} \tau_3, \\
A_3^\pm &= \frac{eg_{KN\Theta} F_1(s)}{s - M^2} \frac{\kappa_N}{M}, \\
A_4^\pm &= \frac{eg_{KN\Theta} F_2(u)}{u - M_\Theta^2} \frac{\kappa_\Theta}{M_\Theta}, \quad (4)
\end{aligned}$$

except for the coupling constant $g_{KN\Theta}$ different between the two parities of Θ^+ . In Eq. (4), $\kappa_p = 1.79$ together with $X = (s - M^2)$ are taken for $\gamma p \rightarrow \bar{K}^0 \Theta^+$, and $\kappa_n = -1.91$ with $X = (t - m_K^2)$ for $\gamma n \rightarrow K^- \Theta^+$, respectively.

For the t-channel K^* and K_1 exchanges, the invariant amplitude A_i^\pm are given by

$$\begin{aligned}
A_1^\pm &= \frac{G_V^{K^*}}{m} (M \pm M_\Theta) \Delta_{K^*}, \\
A_2^\pm &= 0, \\
A_3^\pm &= \frac{G_V^{K^*}}{m} \Delta_{K^*} \pm \frac{G_V^{K_1}}{m} \Delta_{K_1}, \\
A_4^\pm &= \frac{G_V^{K^*}}{m} \Delta_{K^*} \mp \frac{G_V^{K_1}}{m} \Delta_{K_1}. \quad (5)
\end{aligned}$$

Here the coupling constants are $G_V^{K^*} = g_{K^*K\gamma} g_{K^*K\Theta} F_3(t)/m$, $G_V^{K_1} = g_{K_1K\gamma} g_{K_1K\Theta} F_3(t)/m$ with the arbitrary parameter of the mass dimension, m . Also, $\Delta_{K^*} = 1/(t - M_{K^*}^2 + i\Gamma_{K^*} M_{K^*})$, $\Delta_{K_1} = 1/(t - M_{K_1}^2 + i\Gamma_{K_1} M_{K_1})$ are their propagators respectively.

Before proceeding to analyze the differential cross sections, it is worth examining the behavior of the CGLN amplitudes as functions of the photon energy and scattering angle. For clarity, we will focus on the Born contributions in the following. Figs. 4 and 5 show the results where the strength

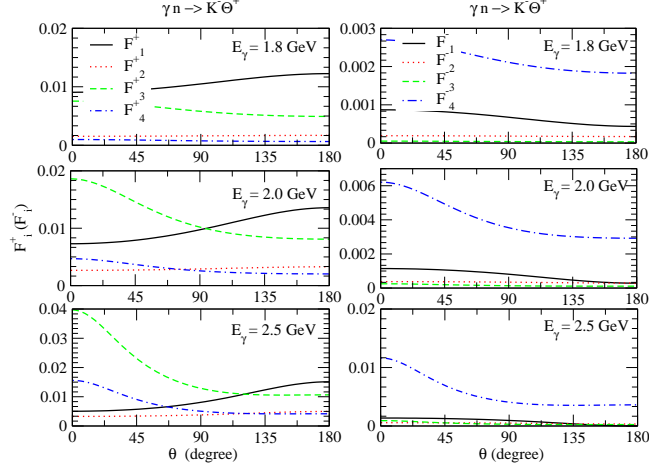


FIG. 4: Angle and energy dependence of the amplitudes F_i^{+} 's for $\Theta^+(\frac{1}{2}^+)$ (left) and F_i^{-} 's for $\Theta^+(\frac{1}{2}^-)$ (right) in the $\gamma n \rightarrow K^- \Theta^+$.

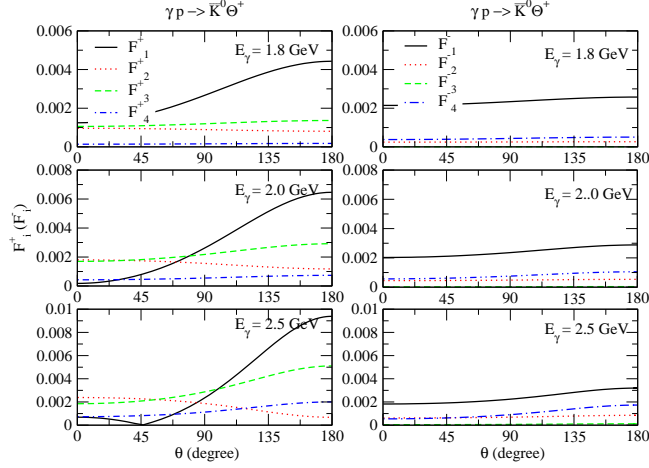


FIG. 5: Angle and energy dependence of the amplitudes F_i^{+} 's for the $\Theta^+(\frac{1}{2}^+)$ (left) and F_i^{-} 's for the $\Theta^+(\frac{1}{2}^-)$ (right) in the $\gamma p \rightarrow \bar{K}^0 \Theta^+$.

of the CGLN amplitudes with Born terms of Eq. (4) are displayed relative to each other. As shown in the figures, the amplitudes F_2^+ and F_4^+ are substantially suppressed near threshold due to the kinematical constant N_- in Eq.(3). Therefore, the current of Eq.(1) near threshold can be written as $\mathbf{J}^+ \cdot \hat{\epsilon}_\lambda \simeq F_1^+ i\boldsymbol{\sigma} \cdot \hat{\epsilon}_\lambda + F_3^+ i\boldsymbol{\sigma} \cdot \hat{\mathbf{k}} \hat{\mathbf{q}} \cdot \hat{\epsilon}_\lambda$. Similarly, the amplitude F_2^- and F_3^- can be neglected near threshold and the current in Eq.(2) can be given by $\mathbf{J}^- \cdot \hat{\epsilon}_\lambda \simeq F_1^- i\boldsymbol{\sigma} \cdot (\hat{\epsilon}_\lambda \times \hat{\mathbf{k}}) + F_4^- \hat{\mathbf{q}} \cdot \hat{\epsilon}_\lambda$. In the process $\gamma n \rightarrow K^- \Theta^+$, the amplitude F_1^+ of the spin-flip term $\boldsymbol{\sigma} \cdot \hat{\epsilon}_\lambda$ known as the Kroll-Ruderman term plays a dominant role over the F_3^+ near threshold in Fig. 4. Beyond the threshold, however, the F_3^+ becomes dominant in the forward direction due to the increase of the t-channel kaon pole

term. For $\Theta^+(\frac{1}{2}^-)$, the amplitude F_4^- is dominant over the others as shown in Fig. 4, because of the kaon pole term with the typical forward angle enhancement. Note that the F_1^- of Kroll-Ruderman term is suppressed relative to the F_4^- in the case of negative parity Θ^+ . This is due to the fact that the contribution of the magnetic interaction term in the amplitude A_1^- of Eq.(4) cancels with the s- and u-channel pole terms and, thus, makes F_1^- small. However, the contributions of the magnetic interaction terms are additive in the A_1^+ to make F_1^+ large in the case of the positive parity.

In the case of $\gamma p \rightarrow \bar{K}^0 \Theta^+$, the process contains only the s- and u-channel pole terms. As shown in Fig. 5, the behaviors of the backward increase are evident for both parities. These are due to the u-channel pole term, producing the angular dependence in that direction. Furthermore, because of the absence of the kaon pole term in this process, the F_1^- in the case of the negative parity dominates all the other amplitudes.

With these in mind, we now analyze the differential cross section. Defining

$$\frac{d\sigma^\pm}{d\Omega} = \frac{|\mathbf{q}|}{|\mathbf{k}|} I^\pm(\theta), \quad (6)$$

$I^\pm(\theta)$ are given by

$$\begin{aligned} I^+(\theta) &= |F_1^+|^2 + |F_2^+|^2 - 2\text{Re}(F_1^{+*} F_2^+) \cos \theta + \sin^2 \theta \\ &\quad \times \left[\frac{1}{2} (|F_3^+|^2 + |F_4^+|^2) + \text{Re}(F_1^{+*} F_4^+ + F_2^{+*} F_3^+ + F_3^{+*} F_4^+ \cos \theta) \right], \\ I^-(\theta) &= |F_1^-|^2 + |F_2^-|^2 - 2\text{Re}(F_1^{-*} F_2^-) \cos \theta + \sin^2 \theta \\ &\quad \times \left[\frac{1}{2} (|F_3^-|^2 \sin^2 \theta + |F_4^-|^2) + \text{Re}(F_1^{-*} F_3^- + F_2^{-*} F_4^- - F_2^{-*} f_3^- \cos \theta) \right]. \end{aligned} \quad (7)$$

Following the above discussions for Figs. 4 and 5, the differential cross sections near threshold can be written as $I^+(\theta) \simeq |F_1^+|^2 + \frac{1}{2} \sin^2 \theta |F_3^+|^2$ and $I^-(\theta) \simeq |F_1^-|^2 + \frac{1}{2} \sin^2 \theta |F_4^-|^2$, respectively.

In Fig. 2, the solid line of the $\frac{d\sigma^+}{d\Omega}$ near threshold, i.e., at $E_\gamma = 1.8$ GeV results from the dominance of the F_1^+ over the F_3^+ as mentioned before and the cross section is governed by $I^+(\theta) \approx |F_1^+|^2$, which produces the typical s-wave behavior. For $\frac{d\sigma^-}{d\Omega}$, the amplitude F_4^- is dominant over the F_1^- as shown in Fig. 4 and the cross section follows $I^-(\theta) \approx \frac{1}{2} \sin^2 \theta |F_4^-|^2$, thus yielding the $\sin^2 \theta$ behavior, a typical p-wave profile as shown in Fig. 2.

In Fig. 3, the solid line of the $\frac{d\sigma^+}{d\Omega}$ near threshold can be understood by the fact that the amplitude F_1^+ becomes larger than F_3^+ gradually in the backward direction as shown in Fig. 5. Therefore, it leads to $I^+(\theta) \approx |F_1^+|^2$ for large angle θ , exhibiting the u-channel angular distribution from F_1^+ . For the $\Theta^+(\frac{1}{2}^-)$, the amplitude F_1^- dominates over F_4^- , which leads to $I^-(\theta) \approx |F_1^-|^2$. Thus, the anticipated p-wave profile from the angle-dependent terms in the

$I^-(\theta)$ is suppressed in the $\frac{d\sigma^-}{d\Omega}$ as shown Fig. 3. Also the u-channel angular distribution is much weakened by the small coupling constant $g_{KN\Theta}$ of the negative parity Θ^+ . These analyses confirm our earlier discussions on Figs. 2 and 3 using the parity and angular momentum conservations.

It is natural to extend our prediction to the polarized photon case and the observation of single polarization observable. Recently, Zhao [17] carried out an analysis of the Θ^+ photoproduction with polarized photon beams using a quark potential model and examined kinematical and dynamical aspects for the purpose of determining Θ^+ 's spin and parity. Since he didn't investigate the kinematic region very close to the threshold as we do in this work let alone his model is different from ours, it is not so easy to make comparisons between his and ours. However, for some cases, we notice that our results are rather close to his results supporting our findings in this work. The asymmetry from the photon polarization (Σ) is defined by an interference between the spin-flip and the spin non-flip transitions, thus enhancing the effect of the small part of the reaction amplitude. In this observable, the properties hidden in the unpolarized characteristics can be revealed.

Following the convention given in Ref. [30], we choose the photon momentum \mathbf{k} in Eqs.(1) and (2) along the z -axis and the vector $\mathbf{k} \times \mathbf{q}$ to be parallel to the y -axis in the center of mass frame of the reaction. Then, the photon polarization asymmetry is defined by

$$\Sigma = \frac{d\sigma/d\Omega^\perp - d\sigma/d\Omega^\parallel}{d\sigma/d\Omega^\perp + d\sigma/d\Omega^\parallel}, \quad (8)$$

where $d\sigma/d\Omega^\perp$ ($d\sigma/d\Omega^\parallel$) is the differential cross section for the photon polarization along x (y) axis.

In terms of the CGLN amplitudes, the Σ for each parity of the Θ^+ is given by

$$\begin{aligned} \Sigma^+ &= -\frac{\sin^2\theta}{2I^+(\theta)} [|F_3^+|^2 + |F_4^+|^2 + 2\text{Re}(F_1^{+*}F_4^+ + F_2^{+*}F_3^+ + F_3^{+*}F_4^+ \cos\theta)], \\ \Sigma^- &= -\frac{\sin^2\theta}{2I^-(\theta)} [|F_3^-|^2 \sin^2\theta + |F_4^-|^2 + 2\text{Re}(F_1^{-*}F_3^- + F_2^{-*}F_4^- - F_2^{-*}F_3^- \cos\theta)], \end{aligned} \quad (9)$$

respectively. The results are given in Figs. 6 and 7. For qualitative understanding, the polarization Σ near threshold can be approximated as $\Sigma^+ \simeq -\frac{\sin^2\theta}{2I^+(\theta)}|F_3^+|^2$ and $\Sigma^- \simeq -\frac{\sin^2\theta}{2I^-(\theta)}|F_4^-|^2$ from Figs. 4 and 5 respectively. Given the differential cross section $I^\pm(\theta)$ in Eq.(9) near threshold as above, we can further write the polarization Σ^+ in Fig. 6 as $\Sigma^+ \approx -\frac{\sin^2\theta}{2|F_1^+|^2}|F_3^+|^2$. Therefore the vanishing polarization, $\Sigma^+ \approx 0$, can be explained substantially by the dominance of the spin-flip transition F_1^+ over the F_3^+ in this energy. The increase of F_3^+ due to the t-channel kaon pole term affects a small deviation of the solid line at $E_\gamma = 2.5$ GeV in the forward angle. On the contrary, the polarization Σ^- in Fig. 6 shows the large negative value of the solid line, stretched strongly toward -1 . This is in sharp contrast to the Σ^+ .

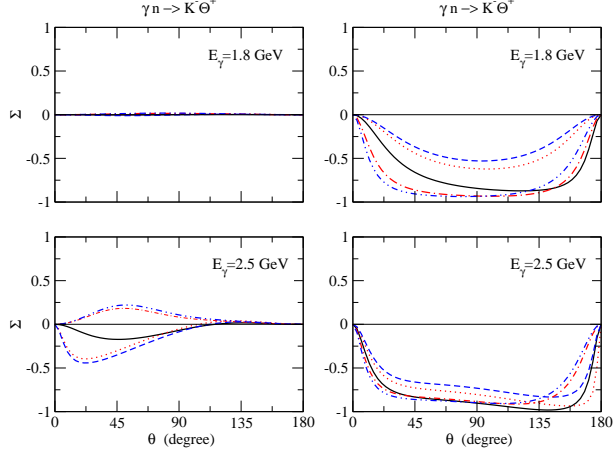


FIG. 6: Polarized photon asymmetries Σ^+ (left) and Σ^- (right) for $\gamma n \rightarrow K^- \Theta^+$ at $E_\gamma = 1.8$ and 2.5 GeV. The notations are the same as Fig. 1.

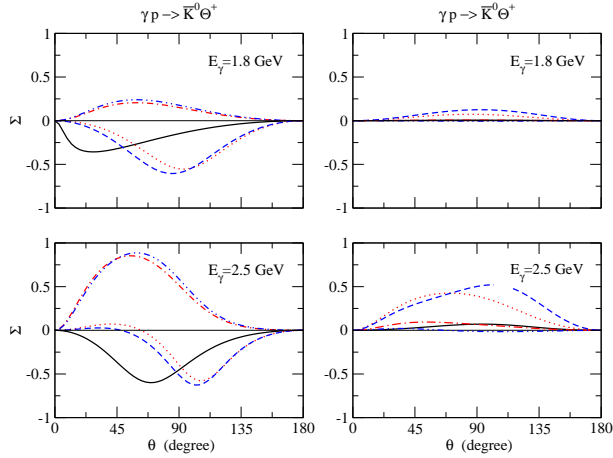


FIG. 7: Polarized photon asymmetries Σ^+ (left) and Σ^- (right) for $\gamma p \rightarrow \bar{K}^0 \Theta^+$ at $E_\gamma = 1.8$ and 2.5 GeV. The notations are the same as Fig. 1.

To understand such a structure, the dominance of the F_4^- over the spin-flip term F_1^- due to the t-channel kaon pole is crucial, i.e., $\Sigma^- \simeq -\frac{\sin^2 \theta}{2 \times \frac{1}{2} \sin^2 \theta |F_4^-|^2} |F_4^-|^2 \simeq -1$. In brief, the polarization Σ for $\gamma n \rightarrow K^- \Theta^+$ near threshold can be characterized by the fact that $\Sigma^+ \approx 0$ due to the dominance of the Kroll-Ruderman term, whereas $\Sigma^- \approx -1$ due to the t-channel kaon pole term. Such trends are not altered much even in the case of including the K^* and K_1 contributions. Therefore, it should be remarked that these contrasting features for the $\gamma n \rightarrow K^- \Theta^+$ make the two opposite Θ^+ parities clearly distinguishable. The result of the Σ^+ in Fig. 6 is in good agreement with that of Ref. [17](Fig.4 of the reference). However, there is some difference in the case of the negative parity.

For the $\gamma p \rightarrow \bar{K}^0\Theta^+$, the situation is somewhat less clear. Nevertheless, the persistence of the Born contributions (solid line) to the $\Sigma^- \approx 0$ up to $E_\gamma = 2.5$ GeV in Fig. 7 deserves to be noticed. Indeed, the null polarization Σ^- in Fig. 7 can be understood by the fact that F_1^- is dominant over F_4^- even if the energy increases as shown in Fig. 5. This nature yields $\Sigma^- \simeq -\frac{\sin^2\theta}{2|F_1^-|^2}|F_4^-|^2 \approx 0$ and sustains such a feature in the solid lines up to $E_\gamma = 2.5$ GeV.

For the K^* and K_1 contributions in Figs. 6 and 7, it is interesting to see that the Σ^+ responds sensitively to the signs of coupling constants, $g_{K^*N\Theta}$ and $g_{K_1N\Theta}$, in both cases of the processes, $\gamma n \rightarrow K^-\Theta^+(\frac{1}{2}^+)$ and $\gamma p \rightarrow \bar{K}^0\Theta^+(\frac{1}{2}^+)$. However, the Σ^- 's for both processes $\gamma n \rightarrow K^-\Theta^+(\frac{1}{2}^-)$ and $\gamma p \rightarrow \bar{K}^0\Theta^+(\frac{1}{2}^-)$ do not change their signs according to the signs of the K^* and K_1 . These asymmetric behaviors of the K^* and K_1 may be due to their enhancement or cancellation within the amplitudes for each parity and in the case of the K^* contributions to the Σ^\pm our results are consistent with Ref. [17].

In summary, based on the CGLN amplitudes and the parity and angular momentum conservation laws, we have analyzed the differential cross sections and the photon polarization asymmetry for $\gamma N \rightarrow K\Theta^+$ near threshold. In particular, the features of the differential cross sections $\gamma n \rightarrow K^-\Theta^+$ near threshold are remarkably consistent with the predictions of the conservation laws of parity and angular momentum. This uniqueness can already be expected from the first principle and thus signifies the model independence of our results. As we demonstrated further, the photon polarization asymmetry Σ can, in principle, also reveal the distinctions between the two parity states of Θ^+ by showing significantly contrasting features with its minimum and maximum polarizations between the two parities in the case of $\gamma n \rightarrow K^-\Theta^+$. Furthermore, the very model dependent K^* and K_1 contributions do not change substantially such features of the Σ . We thus conclude that incorporating the contrasting features of the Σ^\pm for $\gamma n \rightarrow K^-\Theta^+$, the angular distributions near threshold provide an effective tool to determine the Θ^+ parity unambiguously.

Acknowledgments

This work was supported in part by a grant from the U.S. Department of Energy (DE-FG02-96ER 40947).

[1] LEPS Collaboration, T. Nakano *et al.*, Phys. Rev. Lett. **91**, 012002 (2003).

- [2] SAPHIR Collaboration, J. Barth *et al.*, Phys. Lett. B **572**, 127 (2003).
- [3] CLAS Collaboration I, S. Stepanyan *et al.*, Phys. Rev. Lett. **91**, 252001 (2003).
- [4] CLAS Collaboration II, V. Kubarovsky *et al.*, Phys. Rev. Lett. **92**, 032001 (2004).
- [5] DIANA Collaboration, V. V. Barmin *et al.*, Phys. Atom. Nucl. **66**, 1715 (2003).
- [6] A. E. Asratyan, A. G. Dolgolenko, and M. A. Kubantsev, hep-ex/0309042.
- [7] HERMES Collaboration, A. Airapetian *et al.*, Phys. Lett. B **585**, 213 (2004).
- [8] SVD Collaboration, A. Aleev *et al.*, hep-ex/0401024.
- [9] A. V. Manohar, Nucl. Phys. B **248**, 19 (1984).
D. Diakonov, V. Petrov, and M. Polyakov, Z. Phys. A **359**, 305 (1997).
H. Weigel, Eur. Phys. J. A **2**, 391 (1998).
M. Chemtob, Nucl. Phys. B **256**, 600 (1985).
M. Praszalowicz, Phys. Lett. B **575**, 234 (2003).
- [10] H. G. Juengst, nucl-ex/0312019.
Y. Ohashi, hep-ex/0402005.
- [11] R. Jaffe and F. Wilczek, Phys. Rev. Lett. **91**, 232003 (2003)
D. Borisjuk, M. Faber, and A. Kobushkin, hep-ph/0307370.
C. E. Carlson, C. D. Carone, H. J. Kwee, and V. Nazaryan, Phys. Lett. B **573**, 101 (2003); Phys. Lett. B **579**, 52 (2004).
Fl. Stancu and D. O. Riska, Phys. Lett. B **575**, 242 (2003).
A. Hosaka, Phys. Lett. B **571**, 55 (2003).
L. Ya. Golzman, Phys. Lett. B **575**, 18 (2003); hep-ph/0309092.
M. karliner and H. J. Lipkin, Phys. Lett. B **575**, 249 (2003).
E. Shuryak and I. Zahed, hep-ph/0310270.
- [12] S.-L. Zhu, Phys. Rev. Lett. **91**, 232002 (2003).
R. D. Matheus, F. S. Navarra, M. Nielsen, R. da Silva, and S. H. Lee, Phys. Lett. B **578**, 323 (2003).
J. Sugiyama, T. Doi, and M. Oka, Phys. Lett. B **581**, 167 (2004).
F. Csikor, Z. Fodor, S. D. Katz, and T. G. Kovács, JHEP 0311, 070 (2003); hep-lat/0309090.
S. Sasaki, hep-lat/0310014.
- [13] B. G. Yu, T. K. Choi, and C.-R. Ji, nucl-th/0312075, to appear in Phys. Rev. C.
- [14] W. Liu and C. M. Ko, Phys. Rev. C **68**, 045203 (2003)
- [15] W. Liu and C. M. Ko, and V. Kubarovsky, Phys. Rev. C **69**, 025202 (2004).
- [16] Y. S. Oh, H. C. Kim, and S.-H. Lee, Phys. Rev. D **69**, 014009 (2004).
- [17] Q. Zhao, Phys. Rev. D **69**, 053009 (2004).
- [18] Q. Zhao and J. S. Al-Khalili, Phys. Lett. B **585**, 91 (2004).
- [19] K. Nakayama and W. G Love, hep-ph/0404011.
- [20] S.-I. Nam, A. Hosaka, and H.-Ch. Kim, Phys. Lett. B **579**, 43 (2004); hep-ph/0403009.
- [21] S. Nussinov, hep-ph/0307357.

- [22] R. A. Arndt, I. I. Strakovsky, and R. L. Workman, nucl-th/0311030.
- [23] F. E. Close, and Q. Zhao, hep-ph/0403159.
- [24] S.-I. Nam, A. Hosaka, and H.-Ch. Kim, hep-ph/0403009.
- [25] A. W. Thomas, K. Hicks, and A. Hosaka, Prog. Theor. Phys. **111**, 291 (2004).
- [26] <http://pdg.lbl.gov/pdg.html>
- [27] R. A. Williams *et al.*, Phys. Rev. C **46**, 1617 (1992).
- [28] K. Haglin, Phys. Rev. C **50**, 1688 (1994).
- [29] C. F. Chew, M. L. Goldberg, R. E. Low, and Y. Nambu, Phys. Rev. **106**, 1345 (1957).
- [30] C. G. Fasano, F. Tabakin, and B. Saghai, Phys. Rev. C **46**, 2430 (1992).